Shape-sensing motility of cell clusters and collective durotaxis

Author: Àlex Jiménez Becerra*
Master en Física dels Sistemes Complexos i Biofísica.
Facultat de Física, Universitat de Barcelona, Martí i Franquès 1, 08028 Barcelona, Spain.†

Advisor: Jaume Casademunt Viader
Facultat de Física, Universitat de Barcelona, Martí i Franquès 1, 08028 Barcelona, Spain.
Universitat de Barcelona Institut of Complex Systems (UBICS), 08028, Barcelona, Spain.
(Dated: June 30, 2025)

Abstract:
Collective cell migration plays a central role in many biological processes, such as embryonic development, wound healing and cancer progression. Recent studies have predicted that non-circular epithelial cell clusters could collectively migrate through a shape-sensing mechanism, independently of any guiding external cues. This phenomenon has been called 'shape-sensing spontaneous motility' and has been demonstrated in numerical simulations based on the equations for active polar gels adapted to a free-boundary problem, and partially in experiments. On the other hand, collective durotaxis is a well-established phenomenon that manifests in the migration of cell clusters towards stiffer regions when the environment exhibits a stiffness gradient. In this study, we aim to observe and characterise the behaviour of simulated clusters when these two mechanisms are combined and may compete. To address this problem at a quantitative level and in different parameter regimes, one must rely on numerical simulations. Using a code based on the finite elements method, we have modelled the dynamics of cell clusters of different shapes and sizes with or without the effect of durotaxis. Results can then be analysed to draw meaningful conclusions about the motility of these cell clusters and the interplay between the two guiding effects. We find that most cases are highly non-trivial and we find some unexpected behaviours. In addition, we perform a theoretical analysis of the model for the circular case, where the radial symmetry allows us to obtain explicit expressions for most of the magnitudes in the problem. Finally, we study some particular questions arising from simulations, related to the mixed effect of the shape of the clusters and the durotaxis. After our studies, we see that cell clusters are very complex systems where the balance between forces gives rise to intricate and surprising dynamical behaviours. Many cases are not intuitive, but a certain control over the motility of these clusters seems to be possible.

I. INTRODUCTION

Collective cell migration in tissues is essential for understanding a wide variety of biological processes, from embryonic development to fatal diseases [1], [2], [3]. Thus, the direction of cell clusters is a topic of interest in many subjects and several methods have been developed, including the use of electric fields (electrotaxis), light stimuli (phototaxis) and chemical gradients (chemotaxis) [3], [4], [5], [6]. This induced motility is crucial to understanding how many natural processes occur, usually in very specific ways, giving rise to the complex structures we find in living beings of all kinds. Most of these methods are nowadays well known and they are also very present in leading biomedical research, as they can play an important role when developing treatments for different diseases and medical conditions, including some cancers and immune illnesses [1], [7], [8]. In this paper, we want to focus on two of these processes that can be used to lead cells.

The first one is also very well understood and it is based on the stiffness of the substrate a cell cluster is on. Epithelial tissues (very common in this kind of situation) tend to spread over this substrate, generally in a homogeneous way, but the whole set of conditions can determine the final behaviour of these cells [9], [10]. However, when the stiffness of the substrate is not uniform, it has been observed that large enough cell clusters have a clear tendency to move (on average) to those regions where the stiffness is greater [11]. This phenomenon is called durotaxis and it is related to the traction stress cells exert on the substrate to move [12]. When this substrate is stiffer, both the traction and the friction increase, but hydrodynamic interactions in the system give rise to the preferred movement direction [13], [14], [3], [15].

A much newer and harder-to-model method is the effect the shape of the cell cluster has on its movement. As cells in the boundary of the system tend to expand, moving in a direction perpendicular to the same boundary (the one at which boundary cells polarise), one can imagine that the final spreading will depend on the global shape at every moment. When the cluster is hydrodynamically coupled, interactions between all points in the system allow the more surprising phenomenon of collective motility, of course, only when some kind of asymmetry allows the cluster to find a preferred direction. This second process is still under study, but some experiments have already shown that a certain tendency in clusters

* ajimenbe17@alumnes.ub.edu
† master.complex.biophys@ub.edu

with asymmetric shapes can be observed [16].

The study of these systems can be carried out with different approaches, either by defining single cells or by using a continuous model. We have preferred to use the latter, employing an active polar fluid model as a base for the cell cluster [17], [18]. Notice that most biological details are not taken into account, so we focus on the mechanics of the system [19]. This way, some important analytical results can be obtained, as well as expressions for the basic fields that govern the system's dynamics. Moreover, we can carry out computational simulations to analyse all those cases for which we cannot obtain mathematical expressions. In this case, a finite element method is very suitable and we use a code developed in FreeFEM, a coding language designed for this purpose [20].

In this work, we begin by presenting the model and its basic characteristics, as well as some consequences that can be derived from it. Many of them can only be obtained when the cluster is circular. Then, we explain how simulations are performed and present the results we obtained from them, mixing both durotaxis and different shapes. Finally, we also show some theoretical results obtained for the circular case in order to compare them with the simulations and to assess how far we can go with the analytical study, obtaining expressions for the velocity field in each point of the system.

II. ACTIVE POLAR FLUID MODEL

We model our cell cluster as a two-dimensional compressible fluid with free boundary conditions. We can assume compressibility, as cells can modify their shapes thanks to their actin cytoskeleton and reduce their height to occupy the maximum area in the cluster. This means that the divergence of our velocity field will not generally be zero, $\nabla \cdot \mathbf{v} \neq 0$. Moreover, this fluid has a defined polarity field at each point, representing the polarity each cell acquires when close to the boundary. More specifically, the polarity is defined to point perpendicularly outwards with unit modulus, $\mathbf{p} \cdot \mathbf{n} = 1$, for the edge points, and to decay with a characteristic length, $L_c \equiv \sqrt{\frac{K}{a}}$, called the nematic correlation length, when going inwards. This polarity defines the direction along which each cell performs an active force and its strength. Now, as we stated before, this force will depend on the substrate's stiffness and, to a first approximation, this dependence will be linear, so we can define the traction coefficient, ζ_i, to take account of this effect at each point. On the contrary, we consider a constant friction with parameter ξ, so the force balance is given by [16], [13],

$$\nabla \cdot \sigma - \nabla \Pi = \xi \mathbf{v} - \zeta_i \mathbf{p}. \tag{1}$$

Due to the high compressibility of this fluid, however, we will neglect the pressure term, $\nabla \Pi \simeq 0$.

A. Polarisation field

As we mentioned before, the cells of the cluster have a certain polarisation that determines the force each one exerts and its direction. We also defined the nematic correlation length, which gives us an idea of which parts of the cluster remain effectively polarised and which might have a random polarisation, so their values are zero in our coarse-grained study. If this correlation length is comparable to the cluster's size, there will be a polarised outer rim in which cells are correlated (in polarisation). This is the case we want to study, as it has been proved the be the most interesting for shape-sensing motility.

Moreover, this polarisation field relaxes much faster than the velocity field, meaning that we can suppose it is always a solution of the screened Laplace equation [16], [13],

$$\left(L_c^2 \nabla^2 - 1\right) \mathbf{p} = 0, \tag{2}$$

and it is decoupled from the hydrodynamic evolution of the cluster.

B. Velocity field

To study the velocity field, we first have to consider the stress tensor of the fluid. In our case, it can be expressed in terms of the velocity and the polarisation as [16], [13],

$$\sigma_{\alpha\beta} = \eta \left(\partial_\alpha v_\beta + \partial_\beta v_\alpha\right) - \zeta p_\alpha p_\beta. \tag{3}$$

This stress tensor must satisfy the force balance equation. Assuming we are at low Reynolds numbers, inertia can be neglected, so we only have to consider the active stress, proportional to the polarisation, and the passive friction, proportional to the velocity,

$$\partial_\beta \sigma_{\alpha\beta} = \xi v_\alpha - \zeta_i p_\alpha. \tag{4}$$

Putting all this together, the resulting equation is

$$\begin{aligned} \eta \left(\partial_\beta \partial_\alpha v_\beta + \partial_\beta \partial_\beta v_\alpha\right) = \\ = \zeta \left(p_\beta \partial_\beta p_\alpha + p_\alpha \partial_\beta p_\beta\right) + \xi v_\alpha - \zeta_i p_\alpha \end{aligned} \tag{5}$$

or, in vectorial notation,

$$\eta \left[\nabla \left(\nabla \cdot \mathbf{v}\right) + \nabla^2 \mathbf{v}\right] = \zeta \nabla \left(\mathbf{pp}\right) + \xi \mathbf{v} - \zeta_i \mathbf{p}. \tag{6}$$

Notice that, when considering durotaxis, the coefficient of the last term ζ_i, will have a spatial dependence, which one can tune to explore different behaviours.

To complete the model, we need to take boundary conditions into account. In our case, we consider stress-free boundary conditions, which consist of the normal component of the stress vanishing at the boundary [16],

$$\sigma : \hat{\mathbf{n}}\hat{\mathbf{n}} = 0. \tag{7}$$

The model is then defined by equations (2), (6) and (7).

III. ANALYTICAL STUDY OF THE MODEL

A. Polarisation field

The polarisation field can be easily obtained when considering a circular geometry, as it is decoupled from the velocity. Assuming radial symmetry, this polarisation will only have a radial component and will only depend on the radial coordinate. Mathematically,

$$\mathbf{p} = p\left(r\right)\hat{\mathbf{r}}. \tag{8}$$

Equation (2) is then

$$r^2\frac{\partial^2 p}{\partial r^2} + r\frac{\partial p}{\partial r} - \left(\frac{r^2}{L_c^2}+1\right)p = 0, \tag{9}$$

which is a modified Bessel equation of order one. Its general solution is a linear combination of modified Bessel functions of the first and second kind, but, as the latter diverge at the origin, we only keep the former.

Finally, we have to take into account the boundary condition for the polarity, which is simply

$$\mathbf{p}\left(r=R\right) = \hat{\mathbf{n}}, \tag{10}$$

meaning that it is perpendicular to the cell cluster's boundary and has modulus one.

The solution of the polarity field is then

$$p\left(r\right) = \frac{I_1\left(\frac{r}{L_c}\right)}{I_1\left(\frac{R}{L_c}\right)}. \tag{11}$$

This expression will be the same in all cases as long as we consider a circular geometry.

B. Velocity field

As we did with the polarisation, we can aim to obtain an expression for the velocity field when considering a circular geometry, where there is only a radial component and dependence,

$$\mathbf{v} = v\left(r\right)\hat{\mathbf{r}}. \tag{12}$$

Equation (6) then reduces to

$$\eta\left(2\frac{\partial^2 v}{\partial r^2} + \frac{1}{r}\frac{\partial v}{\partial r} - \frac{2}{r^2}v\right) - \xi v = \\ = \zeta\left(2p\frac{\partial p}{\partial r} + \frac{p^2}{r}\right) - \zeta_i p. \tag{13}$$

We can now define the screening length, which accounts for the range of hydrodynamic interactions in our fluid, as

$$\lambda \equiv \sqrt{\frac{2\eta}{\xi}}, \tag{14}$$

so our equation can also be written as

$$\lambda^2\left(\frac{\partial^2 v}{\partial r^2} + \frac{1}{2r}\frac{\partial v}{\partial r} - \frac{1}{r^2}v\right) - v = \\ = \frac{\zeta}{\xi}\left(2p\frac{\partial p}{\partial r} + \frac{p^2}{r}\right) - \frac{\zeta_i}{\xi}p. \tag{15}$$

From now on, our theoretical studies and results will be derived from these equations.

IV. MODEL ANALYSIS AND DISCUSSION

A. Wetting transition

A crucial issue when dealing with epithelial tissues is whether they expand or contract under certain conditions. If the tissue expands, we say it wets, an analogous case to that where adhesion forces between a liquid and the substrate are strong enough to allow the fluid to spread. Conversely, if it contracts, the tissue dewets, meaning it tends to shrink and occupy a smaller surface area on the substrate. It is important to recall that compressibility is a key feature of our fluid. Mathematically, this behaviour is captured by the sign of the velocity field at the edge of the cell cluster.

We now focus on the limiting case, referred to as the wetting transition, the set of conditions under which the tissue neither expands nor contracts [9]. By setting the velocity to zero at $r = R$, we obtain the mathematical condition for the transition,

$$\eta\left(2\left.\frac{\partial^2 v}{\partial r^2}\right|_{r=R} + \frac{1}{R}\left.\frac{\partial v}{\partial r}\right|_{r=R}\right) = \\ = \zeta\left(2p\left(R\right)\left.\frac{\partial p}{\partial r}\right|_{r=R} + \frac{p^2\left(R\right)}{R}\right) - \zeta_i p\left(R\right). \tag{16}$$

To obtain a useful expression, we should replace the velocity field derivatives with their expressions. While the first derivative at the edge comes from the stress-free boundary condition, the second derivative can only be obtained from the velocity field expressions. Despite we get this expression further on, it is not valid for this case because it consists of several integrals of modified Bessel functions. This way, we decide to present and use the condition obtained in the wet limit, where the hydrodynamic length tends to infinity, $\lambda \to \infty$, something equivalent to taking friction out, $\xi = 0$. This way, the wetting transition condition obtained by [9] is given by

$$\frac{\zeta R}{2} - 2\zeta_i L_c^2 + \left(\zeta L_c + \zeta_i L_c R\right)\frac{I_0\left(\frac{R}{L_c}\right)}{I_1\left(\frac{R}{L_c}\right)} - \frac{\zeta R}{2}\frac{I_0^2\left(\frac{R}{L_c}\right)}{I_1^2\left(\frac{R}{L_c}\right)} = 0, \tag{17}$$

for the circular case. Solving this equation for R is not analytical, but numerical solutions can be obtained. A cell cluster of the computed size and with radial symmetry would lie at the transition point so, in the ideal case described by the model, it would neither grow nor shrink.

B. Centre of mass velocity

While we have studied the velocity field at each point of the system, we can also derive an expression for the centre of mass velocity in a general case. For an arbitrary shape, results are not analytical, but its value can be expressed in terms of integrals over the entire domain, Ω, with total area A, which can be computed numerically. When considering the whole evolution of the system, these integrals can be computed at each time, with each shape the system has, to get also the temporal profile of this velocity. The movement of the centre of mass of the domain is then given by

$$\mathbf{V}_{CM} = \frac{1}{A}\left[\int_\Omega \mathbf{v} dS + \int_\Omega \mathbf{r}\left(\nabla\cdot\mathbf{v} - \langle\nabla\cdot\mathbf{v}\rangle\right) dS\right], \quad (18)$$

which is fully kinematic, without taking account of polarity or forces [16]. If we want to write it with the polarity, we have the two integrals,

$$\mathbf{V}_{CM} = \frac{1}{A\xi}\int_\Omega \zeta_i \mathbf{p} dS + \frac{1}{A}\int_\Omega (\mathbf{r} - \mathbf{R_{CM}})\,\nabla\cdot\mathbf{v} dS, \quad (19)$$

which are equivalent to each integral in equation (18) [16]. The former retains the movement caused by a stiffness gradient, the durotaxis motility, while the latter is zero only in the circular case, so it is the cause of the spontaneous motility due to shape.

C. Four main motility modes

Once we understand how our model generally works, we can qualitatively study the behaviour of the system when the relevant parameters have certain values. We will distinguish between four general situations or modes, that are related to correlations between the system's elements at hydrodynamic and polarity levels [16]. To characterise each case better, we will relate the hydrodynamic and polarity correlation lengths, λ and L_c, respectively, to the system's characteristic length, L.

- The simplest case is the one where the system is hydrodynamically uncorrelated and the polarity decays very fast from the edges to the centre, meaning it is only not zero at this boundary. In this case, one can observe that the centre of mass velocity remains zero and the boundary simply expands or contracts, each point independently from the others. This means that the shape is not preserved, but each point advances at the same velocity. In this case, we see that $\lambda \ll L$ and $L_c \ll L$.

- The next possible situation to study is that including the hydrodynamic coupling. This correlates each point in the boundary, what means that its advance or regression is not independent but depends on the whole boundary. This makes the system's shape to be preserved, creating a scale invariance in the system. This also means that the centre of mass remains still. Now, $L_c \ll L$ while $\lambda \gg L$.

- More interesting is the case where we consider a finite polarisation length, $L_c \lesssim L$. This implies that the velocity field inside the cluster is not zero or random, but it is correlated to its value at the boundary. With this, an asymmetry in the shape causes some points of the boundary to advance faster than others, which means that there is a centre of mass displacement, $V_{CM} \neq 0$. However, in this case, the whole boundary expands or contracts, so there is not a coherent movement, in spite of the centre of mass velocity.

- Finally, the most interesting mode is the one where there are both hydrodynamic and alignment correlations and contractility is strong enough. The increase in this last parameter allows the fastest boundary region to dominate over the others and pull on from them [8]. This way, the other points in the boundary have a velocity opposite to their polarity. This behaviour occurs in very specific cases, but it leads to coherent cell migration, the most interesting possibility we observed.

These four modes are graphically represented in FIG. 1, where a schematic behaviour of each one can be seen.

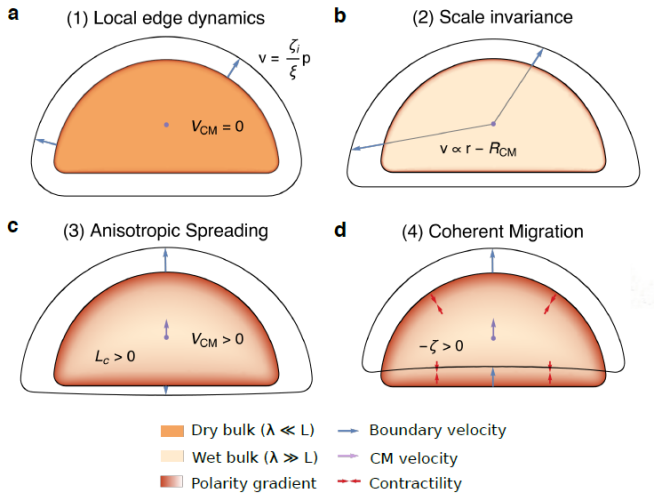

FIG. 1. Schematic representation of the four main modes that are possible for the behaviour of our system for half of a circle. Global characteristics, related to the hydrodynamic and polarity correlation lengths, are represented with the base colour, while velocities and forces are represented with arrows. The centre of mass displacement is only observed in modes three and four, where there are both hydrodynamical and polarisation correlations [16].

D. Divergence and curl decomposition

A very interesting way to study our system and simplify things a bit is to compute the divergence and the curl of our general velocity equation, given by (6), with $\lambda \equiv \sqrt{\frac{\eta}{\xi}}$ (the definition of this length is subject to best possible simplifications),

$$\lambda^2 \left[\nabla (\nabla \cdot \mathbf{v}) + \nabla^2 \mathbf{v}\right] - \mathbf{v} = \\ = \frac{\zeta}{\xi} \left[(\mathbf{p} \cdot \nabla)\, \mathbf{p} + \mathbf{p}\, (\nabla \cdot \mathbf{p})\right] - \frac{\zeta_i}{\xi} \mathbf{p} \equiv \mathbf{P}, \quad (20)$$

where we group the terms with the polarity to a single vector, $\mathbf{P}$, to simplify expressions and calculations. This way, we can easily apply both the divergence and the curl to the equation. The result will also give us the divergence and curl of the velocity field, so we will define

$$\chi \equiv \nabla \cdot \mathbf{v}, \quad (21)$$
$$\omega \equiv (\nabla \times \mathbf{v}) \cdot \hat{\mathbf{z}}, \quad (22)$$

and the equations will then be [16]

$$\left(2\lambda^2 \nabla^2 - 1\right) \chi = \nabla \cdot \mathbf{P}, \quad (23)$$
$$\left(\lambda^2 \nabla^2 - 1\right) \omega = (\nabla \times \mathbf{P}) \cdot \hat{\mathbf{z}}. \quad (24)$$

The divergence of the velocity field essentially contains the information about the spreading of the cluster. This means that the divergence of the polarity terms, $\nabla \cdot \mathbf{P}$, is the source for the spreading rate. On the other hand, the curl equation determines the vorticity of the system and that can be related to the existence of a net movement in a given direction. Its source, $(\nabla \times \mathbf{P}) \cdot \hat{\mathbf{z}}$, is only different from zero when the polarity field, $\mathbf{p}$, does not have radial symmetry (due to the properties of the curl). Moreover, the vorticity field determines the motility mode the system presents. For an asymmetric shape with finite hydrodynamic and polarisation correlation lengths (third and fourth modes), the vorticity profile can propagate matter both upwards and downwards, giving an anisotropic spreading; or do it always upwards, creating a coherent migration (FIG. 2).

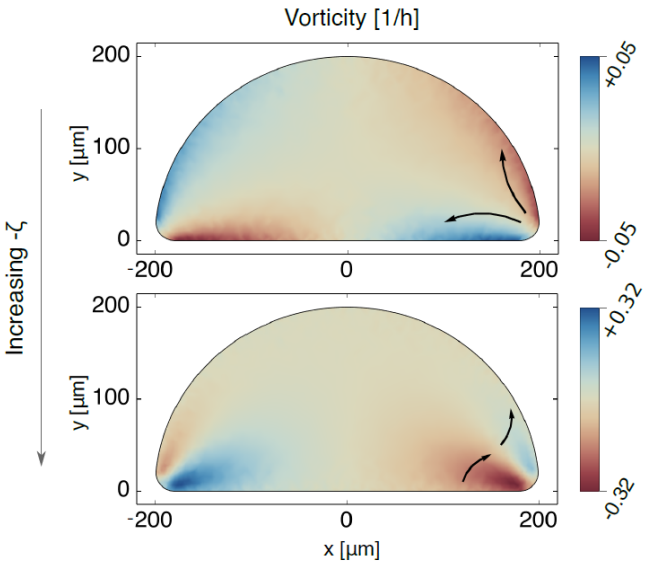

FIG. 2. Vorticity field simulated in a system with a semi-spheric shape, asymmetric with respect to the horizontal axis. In the upside case, vorticity promotes expansion towards all directions, giving rise to an anisotropic spreading. In the other one, vorticity prioritises the flow upwards, giving the coherent migration of the system [16].

V. APPROACH FOR NUMERICAL SIMULATIONS

Numerical simulations presented in this work have been carried out using a program developed in FreeFEM++, a coding language designed for solving systems using the finite element method. In simple terms, the language is structured to define a closed boundary that one has to define, within which a mesh composed of a prescribed number of triangles is automatically generated. In our case, this procedure is repeated at each time step, allowing the domain to evolve according to the computed velocity field.

The main objective of these simulations is to observe the behaviour predicted by the studied model when considering the effects of both durotaxis and the cell cluster's shape. These mechanisms break the symmetry that allows us to easily study the model and possible evolutions of the system, especially when stiffness landscapes are more developed than a straight linear gradient or shapes strongly differ from the circle.

To perform numerical integrations, we first take dimensionality out of it by defining a characteristic length,

$$L \equiv \sqrt{\frac{A}{\pi}}, \quad (25)$$

where A is the system's area, and the characteristic time of a flat front's expansion without contractility like

$$\tau \equiv \frac{\eta}{L_c \zeta_i}. \quad (26)$$

With all this, the polarity field remains the same, $\mathbf{p}' = \mathbf{p}$, while the velocity field is scaled as

$$\mathbf{v}' = \frac{\eta}{L L_c \zeta_i} \mathbf{v}, \quad (27)$$

so the equations we integrate are [16]

$$\nabla'^2 \mathbf{p}' - \left(\frac{L}{L_c}\right)^2 \mathbf{p}' = 0, \quad (28)$$
$$\sigma' = \nabla' \mathbf{v}' + \nabla' \mathbf{v}'^T - \frac{\zeta}{L_c \zeta_i} \mathbf{p}\mathbf{p}, \quad (29)$$
$$\nabla' \cdot \sigma' - \left(\frac{L}{\lambda}\right)^2 \mathbf{v}' + \frac{L}{L_c} \mathbf{p}' = 0. \quad (30)$$

A. Weak form of the equations

These equations, however, have to be written in a weak form to integrate them. When considering the triangular mesh, the polarity equation with the boundary condition, $\mathbf{p}|_{\partial\Omega} = \hat{\mathbf{n}}$, is an inhomogeneous Dirichlet problem that can be written as a homogeneous problem by defining $\mathbf{p_H} = \mathbf{p}' - \mathbf{P_D}$, so

$$\nabla^2 \mathbf{p_H} - \frac{L^2}{L_c^2}\mathbf{p_H} = -\nabla^2 \mathbf{p_D} + \frac{L^2}{L_c^2}\mathbf{p_D} \quad \text{for} \quad \Omega(t), \quad (31)$$

$$\mathbf{p_H} = 0 \quad \text{for} \quad \partial\Omega(t), \quad (32)$$

with $\mathbf{p_D}|_{\partial\omega} = \hat{\mathbf{n}}$

The weak version of equation (31) is, then,

$$\left(\frac{L}{L_c}\right)^2 \int_\Omega \mathbf{p_H}\cdot\mathbf{q}dS + \int_\Omega \nabla\mathbf{p_H}\cdot\nabla\mathbf{q}dS = \\ = -\left(\frac{L}{L_c}\right)^2 \int_\Omega \mathbf{p_D}\cdot\mathbf{q}dS - \int_\Omega \nabla\mathbf{p_D}\cdot\nabla\mathbf{q}dS. \quad (33)$$

The polarity field is then obtained by finding solutions for the components of $\mathbf{p}$ for any test function, $\mathbf{q}$, and adding the $\mathbf{p_D}$ part. All this can be done numerically with specific functions given by the coding language.

We can also obtain the weak version of equation (30) with the new definition of the stress tensor, given by (29), that leads to [16]

$$\int_\Omega \left(\nabla\mathbf{v} + \nabla\mathbf{v}^T\right) : \nabla\mathbf{u}dS + \left(\frac{L}{\lambda}\right)^2 \int_\Omega \mathbf{v}\cdot\mathbf{u}dS = \\ = \frac{L}{L_c}\int_\Omega \mathbf{p}\cdot\mathbf{u}dS + \frac{\zeta}{L_c}\int_\Omega \frac{1}{\zeta_i}\mathbf{pp} : \nabla\mathbf{u}dS, \quad (34)$$

where we have to notice that the traction coefficient is inside the last integral, as we will consider it dependent on space. The problem is again solved by finding the components of the velocity field that satisfy the equation for any test function, $\mathbf{u}$.

B. Shape and size definition

In order to study shapes with different degrees of symmetry, we consider the full circle and new shapes where the lowest part of this circle has been removed. To quantify this, we fix the angular portion, φ, that we take out, which defines a centred portion of the circle facing down. This portion is defined by two radii that meet the circle's boundary at the same height. We can draw a horizontal line uniting these two intersecting points, so the domain below it is removed. Finally, to have a realistic shape and avoid problems deriving from sharp edges, we smooth the resulting angles by drawing circumferences with radii a tenth of the original one. All this process is represented in FIG. 3, where the shaded area is the one removed.

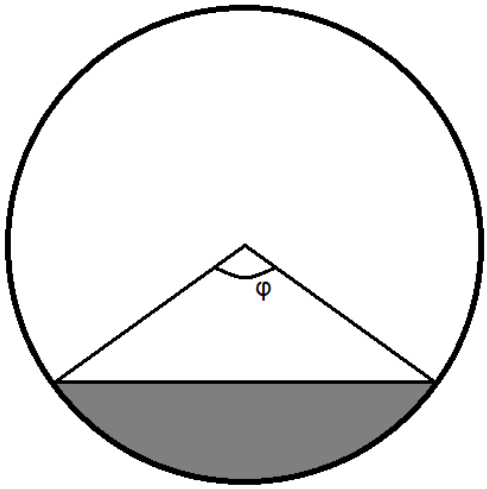

FIG. 3. Schematic representation of how different shapes are crated for the simulations. φ is an angle we fix and the shaded area is removed to get an asymmetric shape.

In our simulations, we will take $\varphi = 0$ (for the complete circle), $\varphi = \frac{\pi}{3}$, $\varphi = \frac{2\pi}{3}$ and $\varphi = \pi$, that is equivalent to a semicircle.

Another measure that we have to define is the radius of this circle. We want our system to begin at the wetting transition, so we can focus on its translation instead of its spreading. By fixing our parameters, the radius is then given by numerically solving equation (17). This is valid, however, to circles only. The easiest way to find an appropriate size for other shapes is just to find the radius that makes the system have the same total area as a circle in the wetting transition would have. This way, the radius for the semicircle is obtained from the wetting transition multiplied by $\sqrt{2}$ and, for a general case, we only need to solve an equation like

$$A_c = A_\varphi \Rightarrow \pi R_c^2 = R_\varphi^2\left(\pi - \frac{\varphi - \sin\varphi}{2}\right) \Rightarrow \\ \Rightarrow R_\varphi = \sqrt{\frac{\pi}{\pi - \frac{\varphi-\sin\varphi}{2}}}R_c, \quad (35)$$

where R_c is the found radius for the circle and R_φ is the radius for a system in the wetting transition with angle φ.

Notice that sizes obtained like this are compatible with clusters formed by a reasonable number of cells.

C. Boundary evolution

When all fields are numerically computed, each triangle vertex in the domain is moved about a distance given by $\mathbf{v}dt$, where the time interval can be chosen to get the desired time resolution. In the mesh definition, the mean distance between the vertices of a triangle is a defined number, h. The displacement of each vertex is kept

under this value to avoid extreme domain deformations. After, this process, we get a new boundary and a new mesh is defined, giving us a new domain to work with.

This iterative process can be extended for an arbitrary number of steps, giving us a collection of labelled boundaries, $\partial\Omega^n$, domains, Ω^n, and fields ordered in time. With all together, one can obtain a fairly long simulation. However, as surface tension and curvature effects are not introduced in the model, resulting shapes after a certain number of iterations are not realistic and simulations become not representative after the corresponding time.

Another thing we have to consider is that the boundary is approximated by a polygonal structure when building the mesh. This means that the normal component of the velocity is not well defined at the vertices and there might be a systematic deviation from the real solution proposed by the model. To correct this, the normal vector at each vertex, i, is defined as

$$\mathbf{n_i} = \frac{1}{1/l_1 + 1/l_{-1}} \left(\frac{\hat{\mathbf{n}}_\mathbf{1}}{l_1} + \frac{\hat{\mathbf{n}}_{-\mathbf{1}}}{l_{-1}} \right), \tag{36}$$

where l_{-1} and l_1 are the previous and posterior edge length, respectively and $\hat{\mathbf{n}}_{\pm\mathbf{1}}$ are the corresponding normal vectors. This vector can be easily normalised, so each normal direction is finally obtained at each vertex too without systematic biases.

Once we finish a simulation, we can also compute other properties of the system to quantify how it has evolved along the whole process. The velocity and traction fields are computed at all points and all times, so their evolutions are well characterised. Moreover, the centre of mass displacement and velocity are also obtained. These magnitudes are crucial to see whether there is a net displacement of the cluster or not. Its position is simply obtained by integrating over the whole domain, while its velocity can be computed from equation (18) with numerical integration. The area change is also an important measure, as it determines if the simulated cells wet or dewet the substrate. Finally, the moments of inertia can also be computed to have a mathematical reference of the shape's evolution, as a great difference between these moments in the x and y axes represents an asymmetry in it, which can also increase or decrease.

D. Post-processing

Once simulations are done, we use a code of Wolfram-Mathematica developed by [16] to compute the different variables we study and plot the graphics of the system's evolution, as well as the animations where this evolution is easily observed. Numerically computing the integrals of the model, all results we want are obtained.

VI. RESULTS FROM SIMULATIONS

We present now the evolutions obtained from the simulations described above. We focused on simulations where durotaxis and shape asymmetry both have effective contributions in the same direction, cooperating in the same sense or competing in opposite senses. An example of the systems we model can be seen in FIG.4, where both the velocity and the traction (directly related to the polarity) fields can be seen for a non-symmetric shape. A whole simulation is given by the evolution of these fields and the boundary where they are defined.

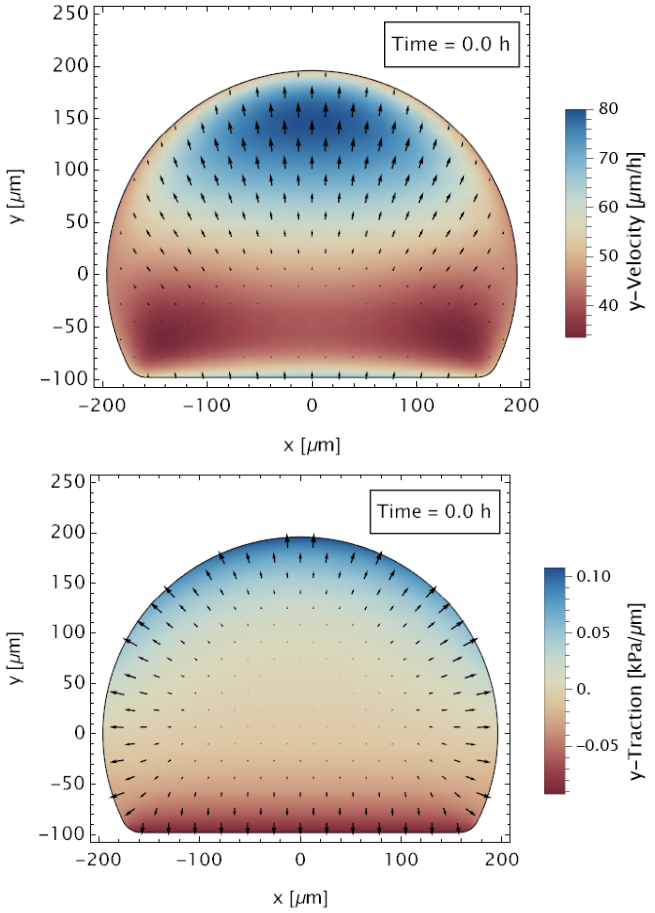

FIG. 4. Example of the velocity (top) and traction (bottom) fields we represent in simulations, for a cluster with $\varphi = \frac{2\pi}{3}$ at its initial time.

A. Systems without durotaxis

First of all, we can see a circular model without durotaxis, where we only observe a change in area due to the traction exerted by the cells at the boundary. This is the basic situation we take as a known model, from which we study the more complex systems we aim to understand. The same study can be done with different shapes and

without durotaxis, observing that an increasing asymmetry leads to a stronger effect of the shape. FIG. 5 shows the evolution of the centre of mass velocity for four different cases, as well as the traction (dashed lines) and spread (dotted lines) integrals The centre of mass displacement and the evolution of the area (relative to its original value) and the moments of inertia are shown in the appendix in FIG. A1.

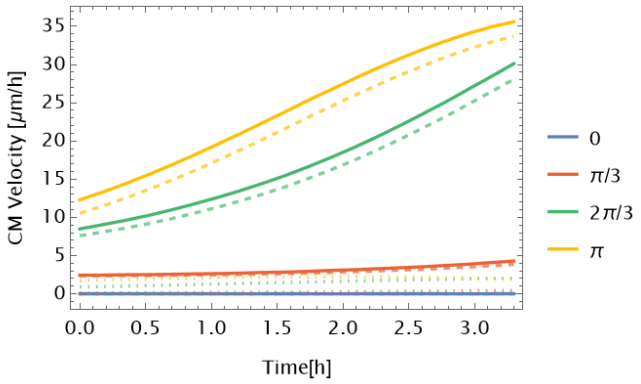

FIG. 5. Evolution of the centre of mass velocity of simulated cell clusters with four different shapes (solid lines). Traction (dashed lines) and spread (dotted lines) integrals are also plotted. These simulations are run without durotaxis.

In this case, we can see how a more asymmetric system experiences a stronger shape effect, advancing further and faster than a more symmetric one. Moreover, despite parameters being set for all systems to be close to the wetting transition, the semicircle ($\varphi = \pi$) quickly shrinks. This is also due to the shape change caused by the system's evolution. This reshaping can be seen in the evolution of the moments of inertia with respect to each other, as their relative values give an idea of how asymmetric is the domain. We can also notice that, for a perfect circle, both moments coincide, while increasing the asymmetry (increasing φ) separates these values. The used parameters are in TABLE I.

B. Systems with durotaxis

Once we incorporate durotaxis into our systems, much more interesting results can arise, depending on the stiffness gradient that is considered. First of all, we are interested in observing how adding a positive gradient (increasing upwards) changes the dynamics of these systems. The centre of mass velocities are shown in FIG. 6 for this case, where one can clearly see that the main change in the behaviour of all systems is that a certain forward velocity has been added. This velocity is approximately constant for the circle, as one can see an almost straight line in the centre of mass position (FIG. 7), while it significantly increases for asymmetric shapes.

The change in the shape of the semicircle, however, is very strong, so the final result becomes not representative. An example of this shape change is seen in FIG. 8, where the final figure is chosen so it is still physically representative. The excessive thinning at the end also explains its dramatic decrease in area and final slowing down (it can be seen in FIG. A2 in appendix). The used parameters are in TABLE I.

The next logical step one may consider is to apply a negative stiffness gradient, so durotaxis and shape effects

TABLE I. Table of parameters used in carried out simulations. Only parameters that we change for different simulations are shown here. Plots of variables in the main text are used to identify simulations.

Simulation figures	φ	R_0 (μm)	ξ (kPa·s/μm^2)	ζ_i' (kPa/μm^2)
FIG. 5	0	175.74	0.1	0
	$\frac{\pi}{3}$	178.33	0.1	0
	$\frac{2\pi}{3}$	195.93	0.1	0
	π	248.54	0.1	0
FIG. 6	0	175.74	0.1	$5 \cdot 10^{-5}$
	$\frac{\pi}{3}$	178.33	0.1	$5 \cdot 10^{-5}$
	$\frac{2\pi}{3}$	195.93	0.1	$5 \cdot 10^{-5}$
	π	248.54	0.1	$5 \cdot 10^{-5}$
FIG. 9	0	175.74	0.1	$-5 \cdot 10^{-5}$
	$\frac{\pi}{3}$	178.33	0.1	$-5 \cdot 10^{-5}$
	$\frac{2\pi}{3}$	195.93	0.1	$-5 \cdot 10^{-5}$
	π	248.54	0.1	$-5 \cdot 10^{-5}$
FIG. 10	π	248.54	0.1	-10^{-5}
FIG. 11	$\frac{2\pi}{3}$	195.93	0.1	$-5 \cdot 10^{-6}$
	π	248.54	0.1	$-5 \cdot 10^{-6}$
FIG. 14	0	175.74	0.1	10^{-4}
FIG. 15	0	175.74	10.0	10^{-4}
	0	175.74	0.1	10^{-4}
FIG. 16	π	248.54	0.1	$-2 \cdot 10^{-5}$
	π	248.54	0.1	$-5 \cdot 10^{-6}$

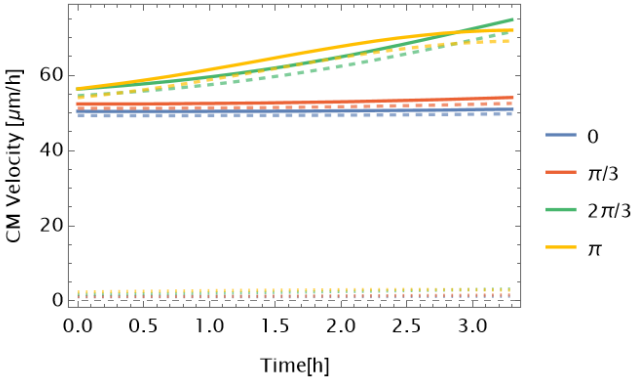

FIG. 6. Evolution of the centre of mass velocity of simulated cell clusters with four different shapes (solid lines). Traction (dashed lines) and spread (dotted lines) integrals are also plotted. A stiffness gradient is applied upwards.

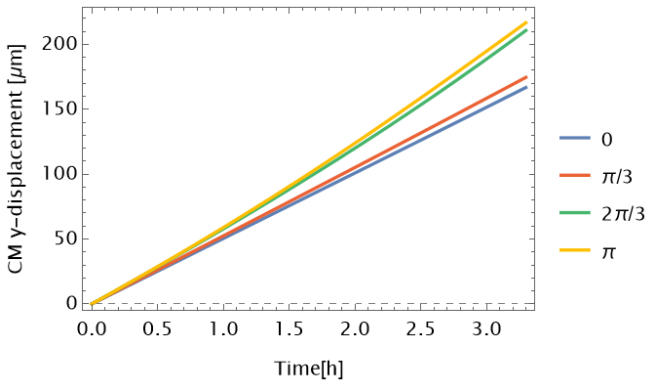

FIG. 7. Evolution of the centre of mass position of simulated cell clusters with four different shapes. A stiffness gradient is applied upwards.

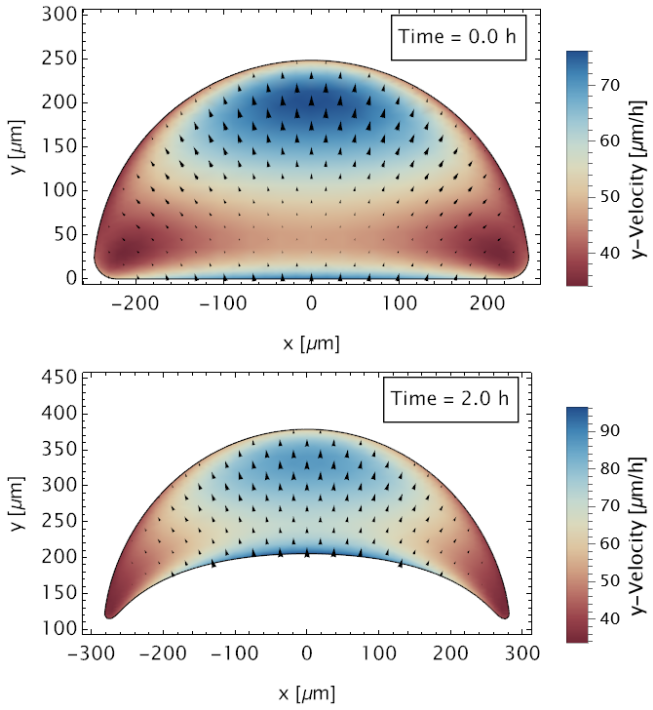

FIG. 8. Change of shape undergone by a cell cluster initially shaped as a semicircle in the presence of durotaxis. The velocity field is also plotted.

would compete with each other. Of course, results show that the shift in velocity is now negative, as one can see in FIG. 9, but it is interesting to see that the semicircle finally reaches the positive velocity and its displacement backwards is relatively small. The vertical displacement, change of area and moments of inertia can be seen in FIG. A3 in the appendix.

The change of shape in the case of the semicircle is similar to the previous one, despite the durotaxis effect being applied in the opposite direction. The used parameters are in TABLE I.

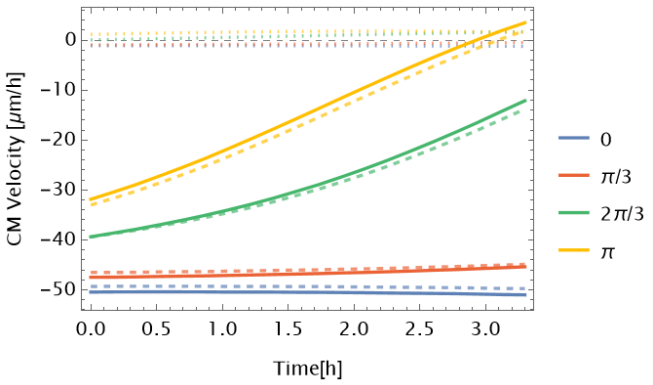

FIG. 9. Evolution of the centre of mass velocity of simulated cell clusters with four different shapes (solid lines). Traction (dashed lines) and spread (dotted lines) integrals are also plotted. A stiffness gradient is applied downwards.

1. *Shape sensing motility vs durotaxis*

A tighter case can be seen when tuning parameters. For a low enough stiffness gradient, the effect of the shape can be stronger than the durotaxis and the centre of mass velocity is still positive (upwards in our simulations). The evolution of this velocity is plotted in FIG. 10, where we see that the system advances in spite of the durotaxis. In the end, it slows down because of the deformation it suffers, but the effect is still clear. This way, we see that the shape-sensing motility is relevant when directing the motion of a cell cluster.

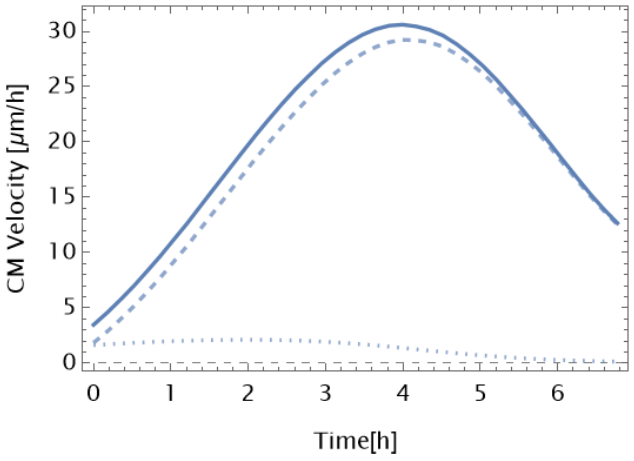

FIG. 10. Evolution of the centre of mass velocity (solid line) for a semicircular cell cluster on a substrate with a downwards stiffness gradient. Traction (dashed line) and spread (dotted line) integrals are also plotted.

We can obtain these results for other shapes. When considering a domain with $\varphi = \frac{2\pi}{3}$ and a small enough downward stiffness gradient, the effect of the shape initially makes the system move forward. Moreover, global

dynamics increases asymmetry, which also increases the effect of the shape. This phenomenon can lead to an enhanced displacement under some conditions, going even further than a semicircular cluster. FIG. 11 shows this case, where the cluster with $\varphi = \frac{2\pi}{3}$ advances more than the one with $\varphi = \pi$ (semicircle), being both over a substrate with the same stiffness gradient. The change of shape can be seen in FIG. 12. The used parameters are in TABLE I.

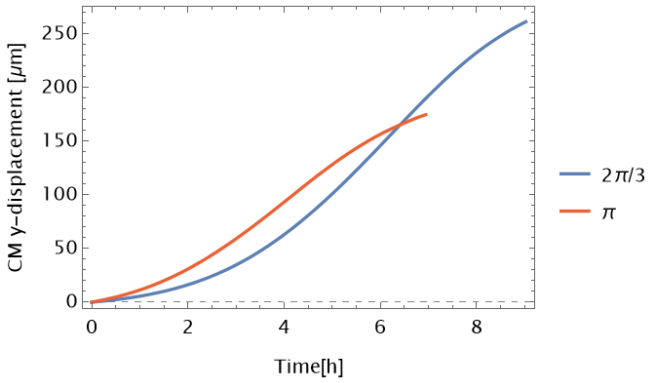

FIG. 11. Evolution of the position of the centre of mass for two cell clusters of different shapes under the effect of durotaxis applied backwards. The simulation of the system with $\varphi = \pi$ ends sooner because it stops being physical before, but it can still be seen how the other system advances further.

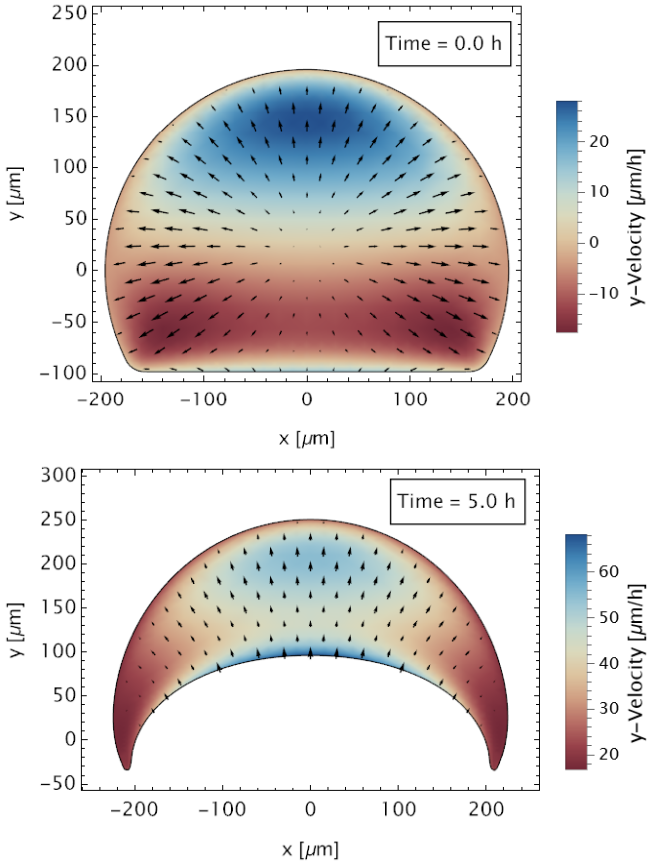

FIG. 12. Change of shape undergone by a cell cluster initially shaped with $\varphi = \frac{2\pi}{3}$ in the presence of durotaxis. The velocity field is also plotted.

C. Preservation of circular symmetry

Another interesting case we can observe in the previous simulations is that the circular system remains circular during the whole simulation. From what we can observe, there doesn't seem to be any deformation, as it is seen in FIG. 13, where only a translation and an expansion occur. Moreover, if we analyse the evolution of the moments of inertia in the x and y axes (FIG. 14), we can see that they coincide at all times, supporting the idea of shape-preserving.

This situation is not very intuitive, as one may think that, being on a stiffer substrate, the front of the cluster would advance faster. However, one has to recall that durotaxis is a collective effect and the whole system has to be considered at all times. Moreover, hydrodynamic couplings might also play a role in shape-preserving. This case shows that possible phenomenologies are difficult to correctly guess without simulations.

The case in the dry limit, where there are only very low-range hydrodynamic interactions, shows much softer durotaxis, so the movement of the cluster is almost zero (apart from its shrinking). This can be seen in FIG. 15, where a comparison with a cluster in the wet limit can be seen for their centre of mass positions. However, as there is no displacement, a change of shape cannot be seen, but the relevance of hydrodynamic interactions becomes also evident for the durotactic effect. This dry limit applies a much stronger friction to the simulation. The used parameters are in TABLE I.

D. Change of shape under durotaxis

Finally, we can also mention that applying different stiffness gradients to a system with the same shape does not affect how this shape evolves very much. In our case, we applied durotaxis with two different intensities to the same system and we could observe how the change in area and moments of inertia was almost the same for both. This means that the geometric evolution of the system is not very sensible to the durotactic effect. These moments of inertia can be seen in FIG. 16, where they almost coincide at all times. The used parameters are in TABLE I.

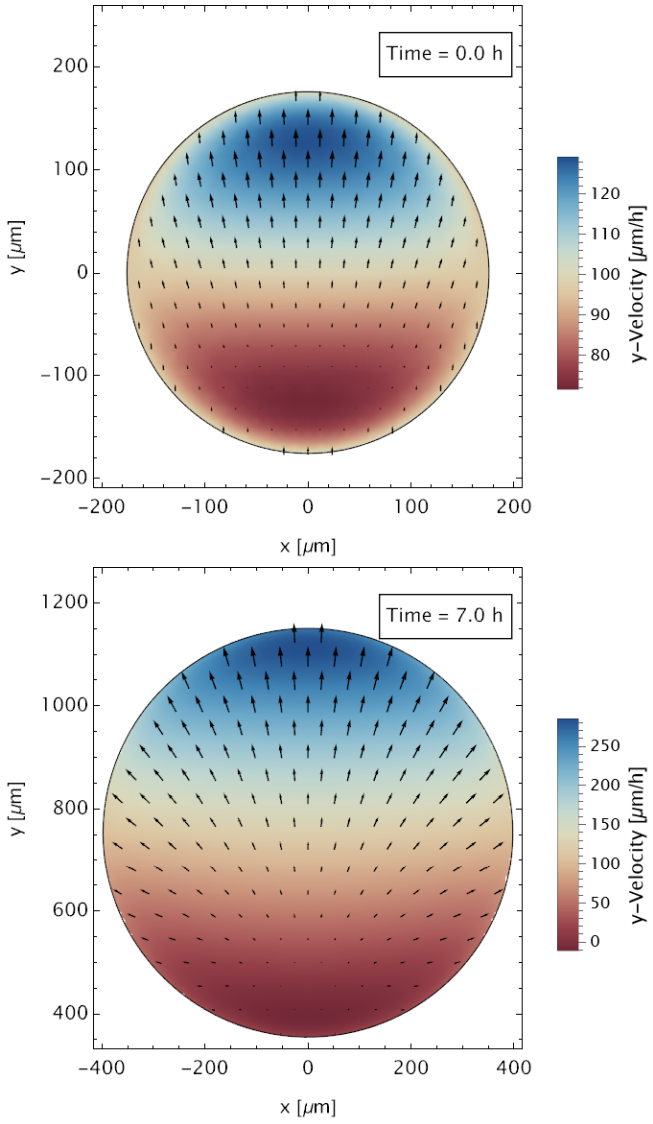

FIG. 13. Circular cell cluster at the beginning (top) and the end (bottom) of a simulation, preserving its shape, in the presence of durotaxis. The velocity field is also plotted.

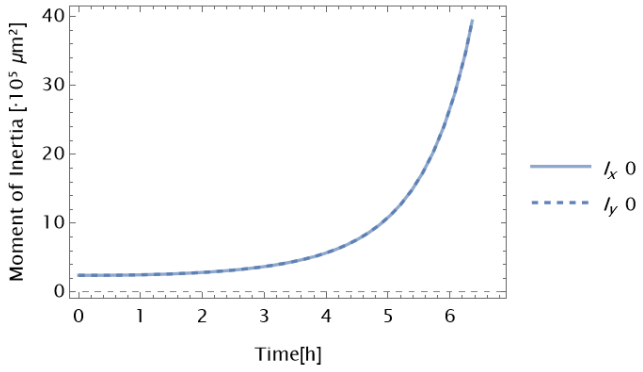

FIG. 14. Moments of inertia in the x (solid) and y axis for a circular cell cluster. Its movement is induced with durotaxis and the system shows spreading, especially at the end of the simulation.

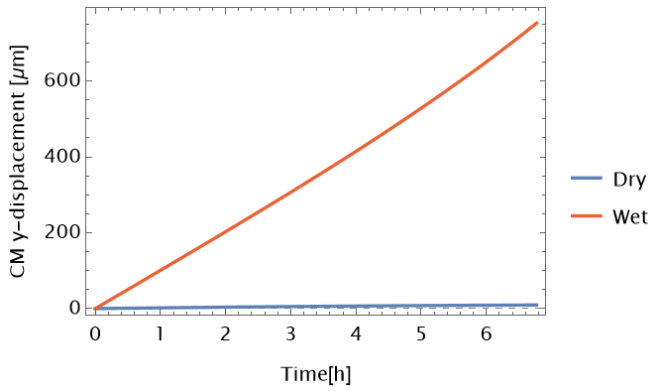

FIG. 15. Evolution of the centre of mass position for two circular clusters with the same initial conditions in the dry and wet limits. A stiffness gradient is applied upwards.

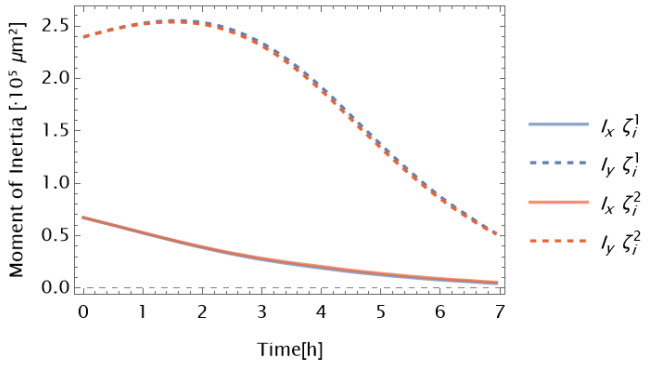

FIG. 16. Moments of inertia for two semicircular cell clusters where different levels of durotaxis are applied downwards, with $\zeta_i^1 = -2 \cdot 10^{-5}$ kPa/μm^2 and $\zeta_i^1 = -5 \cdot 10^{-6}$ kPa/μm^2.

VII. ANALYTICAL RESULTS FOR THE CIRCULAR CASE

A. Solutions and limitations of the velocity field

The homogeneous equation we have can be written like a modified Bessel equation with some small differences,

$$r^2 \frac{\partial^2 v}{\partial r^2} + \frac{1}{2} r \frac{\partial v}{\partial r} - \left(\frac{r^2}{\lambda^2} + 1 \right) v = 0, \tag{37}$$

whose solution can be obtained via the changes of variables $v = r^{\frac{1}{4}} u$ and $x = \frac{r}{\lambda}$, which lead to the expression

$$v_h \left(\frac{r}{\lambda} \right) = A r^{\frac{1}{4}} I_{\frac{\sqrt{17}}{4}} \left(\frac{r}{\lambda} \right) + B r^{\frac{1}{4}} K_{\frac{\sqrt{17}}{4}} \left(\frac{r}{\lambda} \right). \tag{38}$$

In most cases, the constant B will be taken as zero, as modified Bessel functions of the second kind diverge at the origin. However, we will keep it for now to study the particular solution.

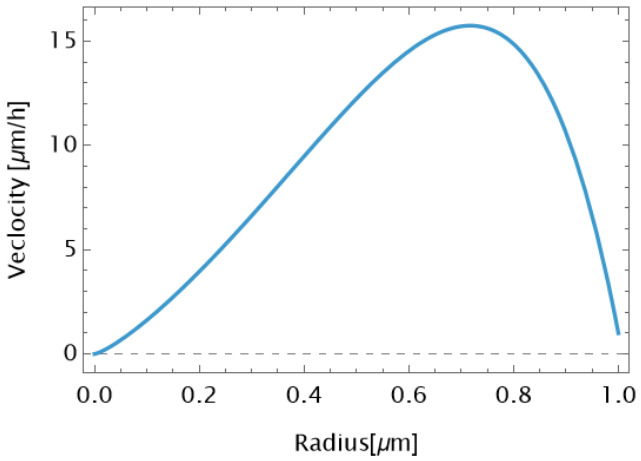

FIG. 17. Velocity profile in terms of the radius for a circular cell cluster without durotaxis.

1. *Particular solution of the circular system*

Unfortunately, we don't have a particular solution for this problem, so everything from now on has to be computed with approximations or numerically. Notice that solutions given in [9] are not valid in this case, as he neglects friction, while this phenomenon is crucial for us.

Nonetheless, we can use the theory on variation of parameters [21] to obtain an expression for the particular solution in term of several integrals of Bessel functions. Beginning with a general expression for this solution,

$$v_p(r) = u_1(r)\, v_1(r) + u_2(r)\, v_2(r), \tag{39}$$

where $u_1(r)$ and $u_2(r)$ are unknown functions and $v_1(r)$ and $v_2(r)$ are each modified Bessel function is the homogeneous solution. By solving the system and integrating it, we can obtain an expression like

$$v_p(r) = -v_1(r)\int \frac{v_2(r)\, f(r)}{W(r)}dr + v_2(r)\int \frac{v_1(r)\, f(r)}{W(r)}dr, \tag{40}$$

where $f(r)$ is the inhomogeneous term of equation (15) and the Wronskian is just

$$W(r) = v_1(r)\, v_2'(r) - v_2(r)\, v_1'(r) = \frac{1}{\sqrt{r}}. \tag{41}$$

This way, a fairly big number of integrals is obtained. The final expression can be found in the appendix, despite it is not used in this paper for any further purpose. As we mentioned, a closed expression cannot be obtained for the particular solution of the velocity field. However, we can use the obtained results to discuss different characteristics of our system. Moreover, the numerical calculation of this solution is in FIG. 17. Notice that this solution is not valid when there is a stiffness gradient.

B. Circular system with durotaxis

As an ansatz, one could imagine that the global velocity field solution when considering durotaxis is a combination of the solution studied before and a centre of mass velocity guided by the stiffness gradient. With this, we would have a global solution like

$$\mathbf{v} = \mathbf{v_0} + \mathbf{v_t}, \tag{42}$$

where $\mathbf{v_0}$ is the velocity field solution of equation (15), which is also solution of equation (6), and $\mathbf{v_t}$ can be written like

$$\mathbf{v_t} = V_{CM}\hat{\mathbf{j}} = V_{CM}\left(\sin\theta\hat{\mathbf{r}} + \cos\theta\hat{\theta}\right), \tag{43}$$

assuming that the stiffness gradient is applied in the $\hat{\mathbf{y}}$ direction.

This approach assumes that the durotactic effect would be a perturbation to the zero-order solution, $\mathbf{v_0}$, which is compatible with the behaviour observed in experiments [12], where durotaxis defines a preferable direction movement for cell clusters, but its effect is relatively small and it can be compared to noise for small enough clusters.

Moreover, this idea implies that the cell cluster preserves its circular shape, so, if the proposed idea is consistent, our equations will be valid at all times, changing only the vertical coordinate, y, along simulations. This has been observed in our simulations also (FIG. 13), as we mentioned in the corresponding section.

We should also consider equation (19) when dealing with this problem, as its result has to coincide with our assumption if it is true. In the simpler case with radial symmetry, the second integral vanishes due to symmetry, while the first can be simplified so the centre of mass velocity is given by

$$V_{CM} = \frac{\pi\zeta_i'}{A\xi}\int_0^R r^2 p(r)\, dr, \tag{44}$$

where we already replaced the traction with its linear expression when considering durotaxis.

Now, to test our hypothesis, we can analyse our equations again. We have to consider that both the Laplacian and the gradient of the divergence of the $\hat{\mathbf{y}}$ vector are zero (notice that this is independent of the coordinates system). This way, introducing our ansatz in equation (6) with a linearly changing traction, we see that

$$\mathbf{v_t} = \frac{\zeta_i'}{\xi}(r - R_{CM})\sin\theta\mathbf{p}. \tag{45}$$

A clear problem arises here. As we see in (43), our assumption for the translational velocity has both radial and angular components, while the polarity field is the only contribution in the equation obtained from the model, but this field is only radial. This way, we have a mathematical restriction of the angle coordinate, which is not possible from a physical point of view. So we can see that the actual case is much more complex.

This result means that the circular shape is not expected to be preserved. Simulations seem to show this symmetry conservation, so the effect of durotaxis in the shape might be very small. Another possibility is that the hydrodynamic coupling given by a large λ avoids a noticeable difference between the velocity of the upper and lower extremes in the circle. More research in simulations might be done to observe compatible results.

VIII. CONCLUSIONS

Our study of the active polar fluid model has given us many different and important results. Some of them are well known and can be used to confirm what others have studied, we have also observed many non-trivial behaviours, some of them never studied before. As a first achieved goal, we have accurately characterised several properties of the studied model, obtaining the basic equations that govern it and developing them for the circular case. More interesting is the general case where we observe how the characteristic lengths of the model determine the global behaviour of the system. From this analysis, we have noticed the importance of contractility for creating a certain vorticity in the fluid, allowing it to show a coherent movement.

Many relevant results we obtained come from simulations. First, we have observed the effect of the shape on the system's dynamics. Under appropriate conditions, the desired migration is observed for asymmetric shapes, increasing the cluster's displacement when its shape is more asymmetric. Semicircular clusters have shown how this effect can be outstanding. This result was already observed by [16], but we also introduced durotaxis. As we expected, a stiffness gradient made all systems advance or go backwards. However, the most interesting result has been obtained from mixing both durotaxis and shape-sensing motility to make them cooperate or compete, showing a huge variety of possible outcomes. Something remarkable has been that, for small enough traction gradients, the shape of the cluster can be enough to make it overcome a negative durotactic effect and advance.

We also have to state some curious phenomena we observed from these simulations. As deformation becomes excessive in non-circular simulations, one has to notice that systems finally reach non-realistic shapes. This points out that some modifications in simulations might be done to avoid these effects. However, assuming that a certain deformation is acceptable, we observed how very asymmetric shapes end up playing the opposite role and slow down the cluster's advance. This way, some more symmetric shapes might be more efficient under some conditions. We also observed how these deformations do not depend very much on the applied stiffness gradient, so they basically are a consequence of the initial shape.

A last interesting result we got from simulations is the fact that a circular cell cluster under the effect of durotaxis remains circular despite its movement and expansion (or shrinkage). This result was not expected and it is assumed to be a result of considering a large hydrodynamical length, λ, that correlates the whole system and allows it to preserve its shape. Analytical results concerning this case have shown, however, that the change in the velocity field due to durotaxis is not just the addition of a translation velocity, but the velocity field globally changes. The only assumption one can make with respect to this problem is that the velocity at the boundary is in some way modified by the addition of this velocity.

Finally, we aimed to obtain a solution for the velocity field in the circular case without durotaxis, which is the only one that preserves the radial symmetry. Reducing our problem to a one-dimensional one, we could obtain all equations that govern the system and obtain explicit analytical solutions until a certain point. Despite the homogeneous equation for the velocity having a known solution, the particular one resulted in several integrals of modified Bessel functions and so, its final expression could not be found. However, we could perform numerical integrals to obtain a graphical functional form compatible with what is observed from simulations. This way, the velocity profile shape could be obtained, something never done before when including friction in the model.

APPENDIX

A. More magnitudes plots

We now present plots of additional properties computed from simulations that were not relevant to our study. FIG. A1 compiles these properties for simulations without durotaxis, while FIG. A2 and A3 show the equivalent plots for the upwards and downwards durotaxis, respectively.

B. Velocity profile expression

To simplify (a bit) notation, we can define integrals of modified Bessel functions like

$$\sigma^{\mu_1(\beta_1),\dots,\mu_n(\beta_n)}_{\nu_1(\alpha_1),\dots,\nu_n(\alpha_n)}(x;\gamma) \equiv \equiv \int I_{\nu_1}(\alpha_1 x)\dots I_{\nu_n}(\alpha_n x)\cdot \cdot K_{\mu_1}(\beta_1 x)\dots K_{\mu_n}(\beta_n x)\, x^{\gamma} dx, \quad \text{(A1)}$$

the particular solution can be written like in equation (A2), but it is still hard to manage and we do not use it.

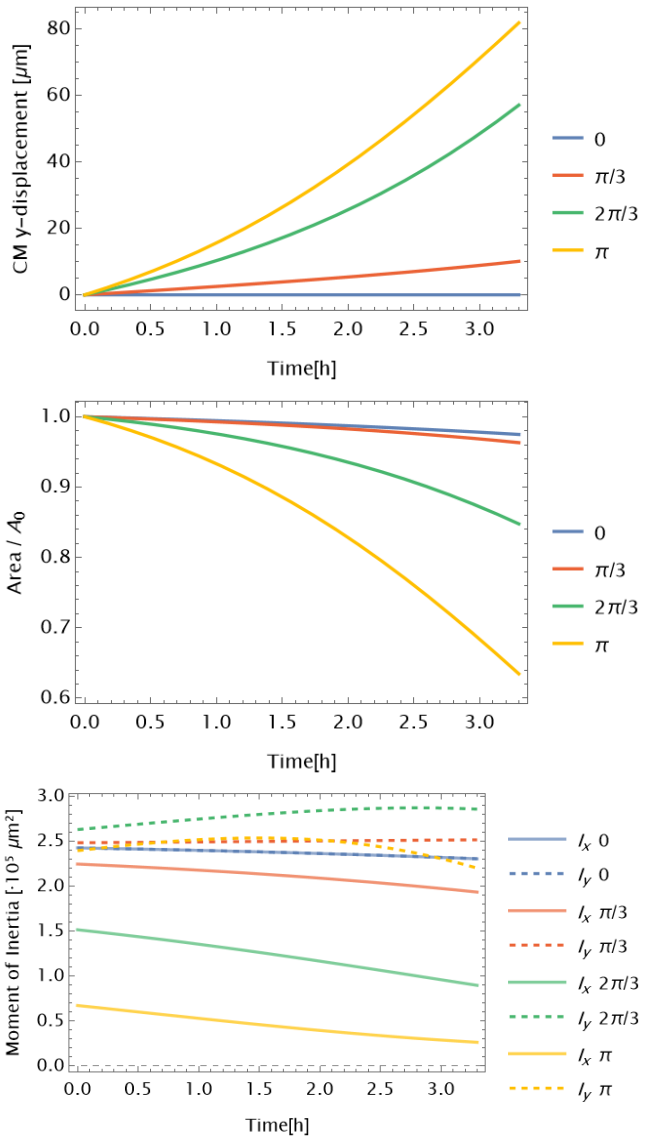

FIG. A1. Evolution of the centre of mass position (top), area (centre) and moments of inertia (bottom) of simulated cell clusters with four different shapes. These simulations are run without durotaxis.

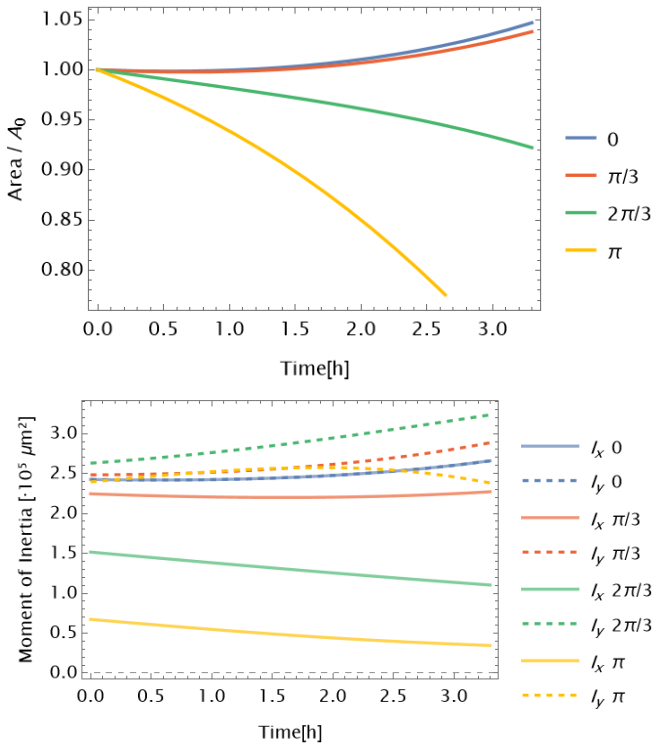

FIG. A2. Evolution of the area (top) and moments of inertia (bottom) of simulated cell clusters with four different shapes. A stiffness gradient is applied upwards.

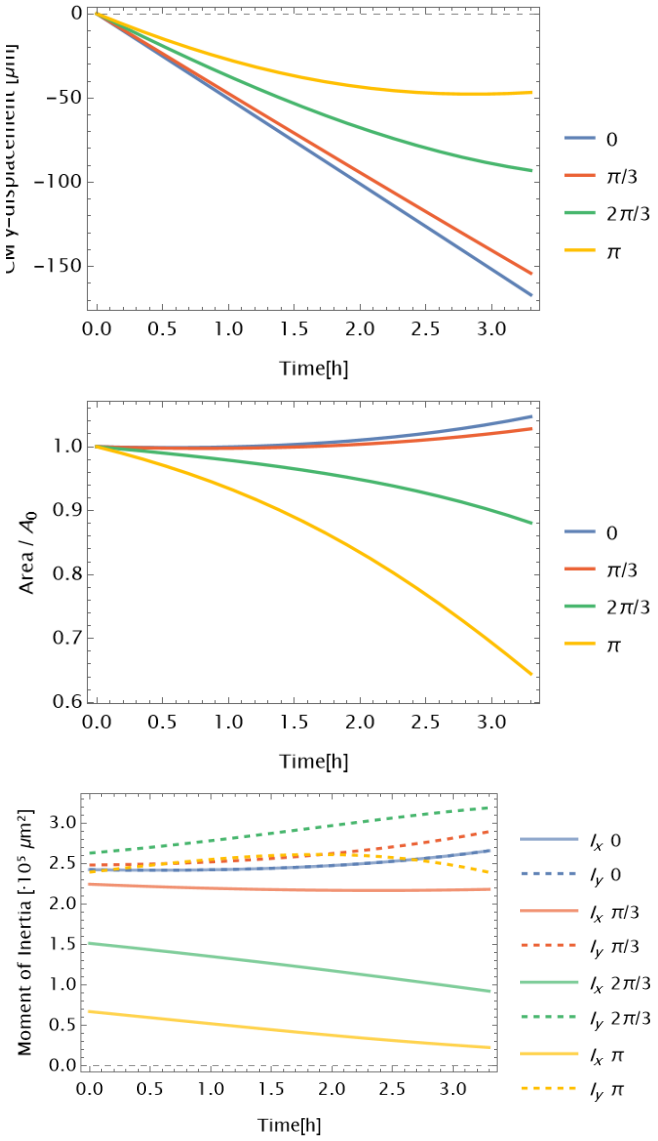

FIG. A3. Evolution of the centre of mass position (top), area (centre) and moments of inertia (bottom) of simulated cell clusters with four different shapes. A stiffness gradient is applied downwards.

$$
\begin{aligned}
v_p(r) = \\
&= \frac{r^{\frac{1}{4}}}{\lambda^2 \xi} \frac{1}{I_1\left(\frac{R}{L_c}\right)} \Bigg[-\zeta \frac{I_{\frac{\sqrt{17}}{4}}\left(\frac{r}{\lambda}\right)}{I_1\left(\frac{R}{L_c}\right)} \left(\frac{1}{L_c} \sigma^{\frac{\sqrt{17}}{4}\left(\frac{1}{\lambda}\right)}_{0\left(\frac{1}{L_c}\right),1\left(\frac{1}{L_c}\right)} \left(r; \frac{11}{4}\right) + \frac{1}{L_c} \sigma^{\frac{\sqrt{17}}{4}\left(\frac{1}{\lambda}\right)}_{1\left(\frac{1}{L_c}\right),2\left(\frac{1}{L_c}\right)} \left(r; \frac{11}{4}\right) + \sigma^{\frac{\sqrt{17}}{4}\left(\frac{1}{\lambda}\right)}_{1\left(\frac{1}{L_c}\right),1\left(\frac{1}{L_c}\right)} \left(r; \frac{7}{4}\right) \right) + \\
&\quad + \zeta_i I_{\frac{\sqrt{17}}{4}}\left(\frac{r}{\lambda}\right) \sigma^{\frac{\sqrt{17}}{4}\left(\frac{1}{\lambda}\right)}_{1\left(\frac{1}{L_c}\right)} \left(r; \frac{11}{4}\right) + \\
&+ \zeta \frac{K_{\frac{\sqrt{17}}{4}}\left(\frac{r}{\lambda}\right)}{I_1\left(\frac{R}{L_c}\right)} \left(\frac{1}{L_c} \sigma_{0\left(\frac{1}{L_c}\right),1\left(\frac{1}{L_c}\right),\frac{\sqrt{17}}{4}\left(\frac{1}{\lambda}\right)} \left(r; \frac{11}{4}\right) + \frac{1}{L_c} \sigma_{1\left(\frac{1}{L_c}\right),2\left(\frac{1}{L_c}\right),\frac{\sqrt{17}}{4}\left(\frac{1}{\lambda}\right)} \left(r; \frac{11}{4}\right) + \sigma_{1\left(\frac{1}{L_c}\right),1\left(\frac{1}{L_c}\right),\frac{\sqrt{17}}{4}\left(\frac{1}{\lambda}\right)} \left(r; \frac{7}{4}\right) \right) - \\
&\quad - \zeta_i K_{\frac{\sqrt{17}}{4}}\left(\frac{r}{\lambda}\right) \sigma_{1\left(\frac{1}{L_c}\right),\frac{\sqrt{17}}{4}\left(\frac{1}{\lambda}\right)} \left(r; \frac{7}{4}\right) \Bigg] . \quad \text{(A2)}
\end{aligned}
$$

ACKNOWLEDGMENTS

I would like to express my sincere gratitude to Doctor Jaume Casademunt for his guidance and support during this work and to Joan Térmens for being so helpful and carrying out the simulations present in this project, for he developed the used code. I also want to thank my family and friends for their constant support during these months and all previous experiences.

[1] P. Friedl and D. Gilmour, "Collective cell migration in morphogenesis, regeneration and cancer" *Nat. Rev. Mole. Cell Biol.* vol. 10, pp. 445-457, 2009.

[2] R. Majumdar et al., "New paradigms in the establishment and maintenance of gradients during directed cell migration" *Curr. Opin. Cell Biol.* vol. 30, pp. 33-40, 2014.

[3] A. Haeger et al., "Collective cell migration: guidance principles and hierarchies" *Trens Cell Biol.* vol. 25, no. 9, 2015.

[4] M. Poukkula et al., "Cell behaviors regulated by guidance cues in collective migration of border cells" *J. Cell Biol.* vol. 192, no. 3, 2011.

[5] B. Camley et al., "Cell behaviors regulated by guidance cues in collective migration of border cells" *Phys. Rev. Lett.* vol. 116, pp. 1-6, 2016.

[6] J. G. Lyon et al., "Electrotaxis of glioblastoma and medulloblastoma spheroidal aggregates" *Sci. Rep.* vol. 9, no. 5309, 2019.

[7] B. J. DuChez et al., "Durotaxis by Human Cancer Cells" *Biophys. J.* vol. 116, pp. 670-683, 2019.

[8] R. Mayor and S. Etienne-Manneville, "The front and rear of collective cell migration" *Nat. Rev. Mole. Cell Biol.* vol. 17, pp. 97-109, 2016.

[9] C. Pérez-González et al., "Active wetting of epithelial tissues" *Nat. Phys.* vol. 15, pp. 79-88, 2019.

[10] R. Alert and J. Casademunt, "Role of Substrate Stiffness in Tissue Spreading: Wetting Transition and Tissue Durotaxis *Langmuir* vol. 35, pp. 7571-7577, 2019.

[11] A. Shellard and R. Mayor, "Collective durotaxis along a self-generated stiffness gradient in vivo" *Nature* vol. 600, pp. 690-694, 2021.

[12] R. Sunyer and X. Trepat, "Durotaxis" *Curr. Biol.* vol. 30, pp. 371-392, 2020.

[13] I. Pi-Jaumà, R. Alert and J. Casademunt, "Collective durotaxis of cohesive cell clusters on a stiffness gradient" *Eur. Phys. J. E* vol. 45, no. 7, 2022.

[14] M. E. Pallarès et al., "Stiffness dependent active wetting enables optimal collective cell durotaxis" *Nat. Phys.* vol. 19, pp. 279-289, 2023.

[15] R. Sunyer et al., "Collective cell durotaxis emerges from long-range intercellular force transmission" *Science* vol. 353, pp. 1157-1161, 2016.

[16] J. Térmens et al., "Shape-sensing spontaneous motility of cell clusters", unpublished.

[17] M. C. Marchetti et al., "Hydrodynamics of soft active matter" *Rev. Mod. Phys.*, vol. 85, no.3, 2013.

[18] R. Alert and X. Trepat, "Physical Models of Collective Cell Migration" *Annu. Rev. Condens. Matter Phys.* vol. 11, pp. 77-101, 2020.

[19] S. R. K. Vedula et al., "Collective Cell Migration: A Mechanistic Perspective" *Physiology* vol. 28, pp. 370-379, 2013.

[20] FreeFEM website. Accessed: 2025 [Online.] Available: https://freefem.org/

[21] W. E. Boyce and R. C. DiPrima, "Second Order Linear Equations" in *Elementary Differential Equations and Boundary Value Problems*, J. Wiley & Sons, Inc., Hoboken, NJ, United States of America, Rosatone, 2009, ch. 3, pp. 185-189.